







Quantitative description of long-range order in the spin- $\frac{1}{2}$ XXZ antiferromagnet on the square lattice

Nils Caci ^{1,2,*}, Dag-Björn Hering ^{3,†}, Matthias R. Walther ^{4,‡}, Kai P. Schmidt ^{4,§},
Stefan Wessel ^{2,||} and Götz S. Uhrig ^{3,¶}

¹*Laboratoire Kastler Brossel, Collège de France, Centre National de la Recherche Scientifique, École Normale Supérieure–Université PSL, Sorbonne Université, 75005 Paris, France*

²*Institute for Theoretical Solid State Physics, RWTH Aachen University, Otto-Blumenthal-Straße 26, 52074 Aachen, Germany*

³*Condensed Matter Theory, TU Dortmund University, Otto-Hahn-Straße 4, 44221 Dortmund, Germany*

⁴*Department of Physics, Friedrich-Alexander-Universität Erlangen-Nürnberg, Staudtstraße 7, 91058 Erlangen, Germany*



(Received 14 May 2024; revised 10 July 2024; accepted 11 July 2024; published 6 August 2024)

The quantitative description of long-range order remains a challenge in quantum many-body physics. We provide zero-temperature results from two complementary methods for the ground-state energy per site, the sublattice magnetization, the spin gap, and the transverse spin correlation length for the spin-1/2 quantum XXZ antiferromagnet on the square lattice. On the one hand, we use exact, large-scale quantum Monte Carlo (QMC) simulations. On the other hand, we use the semianalytic approach based on continuous similarity transformations in terms of elementary magnon excitations. Our findings confirm the applicability and quantitative validity of both approaches along the full parameter axis from the Ising point to the symmetry-restoring phase transition at the Heisenberg point and further provide quantitative reference results in the thermodynamic limit. In addition, we analytically derive the relation between the dispersion and the correlation length at zero temperature in arbitrary dimension, and discuss improved second-moment QMC estimators.

DOI: [10.1103/PhysRevB.110.054411](https://doi.org/10.1103/PhysRevB.110.054411)

I. INTRODUCTION

The collective behavior of matter is one of the most important topics of modern science. Understanding it is crucial in basic research as it holds the key to a variety of correlated many-body states—realized for example in topologically ordered quantum phases such as spin liquids and fractional quantum Hall liquids or superconductors. At the same time, it is clear that this understanding forms the basis for many technological applications such as magnetic data storage [1] and spintronics [2,3] which define the modern era. In particular, it is decisive to gain a systematic and quantitative understanding of collective phenomena.

Quantum magnetism has turned out to serve as a very fruitful playground to study collective quantum phenomena. Indeed, frustrated magnets are known to host a variety of exotic quantum phases such as spin-liquid ground states with topological quantum order. Unfrustrated quantum antiferromagnets with long-range magnetic Néel order play an important role for the physics of high-temperature superconductors [4], because the undoped parent compounds represent two-dimensional antiferromagnetic Heisenberg magnets with $S = 1/2$ on the square lattice [5]. Furthermore, spintronics is a huge field of applications in which the

manipulation of magnetism is crucial [1–3], requiring a fundamental understanding of the underlying mechanisms.

It is very common to describe the magnetic excitations of quantum antiferromagnets by essentially interaction-free magnons [6]. By “essentially free of interactions” we mean that some static renormalization of the dispersions is accounted for, but the magnon-magnon scattering processes are rarely considered quantitatively. Yet it turned out that the interaction of the magnons is very important to understand certain dips (dubbed “roton dips”) in the dispersion [7,8] and the distribution of spectral weight in the continua [9]. This has been shown by establishing a continuous basis change, namely a continuous similarity transformation (CST), such that the number of magnons in the target basis is conserved, at least to very good approximation [7,9,10]. This facilitates the interpretation of the results greatly, for instance the dispersion can be read off immediately. The computation of continua at zero temperature formed from two or three elementary excitations [11] only requires solving a two- or three-particle problem, avoiding complicated diagrammatic techniques. In this fashion, also bound states of two [12–15] or three particles [11] were identified.

To support these calculations and to assess their validity, we turn to static quantities such as the ground-state energy per site e_0 , the sublattice magnetization m^z , the spin gap Δ , and the transverse spin correlation length ξ and compare theoretical results for them stemming from two very different approaches.

One is the above-mentioned CST which maps the original model expressed by magnon creation and annihilation operators to an effective model in magnon operators, but with conservation of the number of magnons. The CST consists in

*Contact author: nils.caci@lkb.ens.fr

†Contact author: dag.hering@tu-dortmund.de

‡Contact author: matthias.walther@fau.de

§Contact author: kai.phillip.schmidt@fau.de

||Contact author: wessel@physik.rwth-aachen.de

¶Contact author: goetz.uhrig@tu-dortmund.de

setting up a general flow equation in all couplings and solving this flow equation. The first step is analytical, the second numerical eventually providing the coupling constants of a magnonic model in second quantization. Thus, we classify this approach as semianalytical. The data for e_0 , Δ , and ξ are already published in Ref. [10].

The second approach involves quantum Monte Carlo (QMC) simulations using the stochastic series expansion (SSE) algorithm with directed loops [16–19], which is a well-established numerically exact method for unbiased, large-scale studies of quantum magnets.

Our paper demonstrates the applicability and quantitative validity of CST and QMC along the full parameter line from the Ising to the Heisenberg model. In particular, we capture the phase transition from the gapped ordered phase at any finite anisotropy to the gapless Heisenberg point with full SU(2) symmetry. Our results confirm that associated critical exponents at this symmetry-restoring phase transition are given exactly by the ones from spin-wave theory.

The paper is set up as follows. In Sec. II we briefly introduce the model and describe the two employed complementary methods concisely with an emphasis on how the particular quantities are computed. The results are presented and discussed in Sec. III. Section IV concludes the paper.

II. MODEL AND METHODS

A. Model

We consider an insulating quantum antiferromagnet with $S = 1/2$ and easy-axis anisotropy defined by the anisotropy parameter $\lambda = J_{xy}/J_z \in [0, 1]$ so that the Hamiltonian takes the form

$$H = J \sum_{\langle i,j \rangle} \left[\frac{\lambda}{2} (S_i^+ S_j^- + S_i^- S_j^+) + S_i^z S_j^z \right] \quad (1)$$

in terms of the spin ladder operators. The model is bipartite and thus unfrustrated. It breaks the \mathbb{Z}_2 symmetry of spin flips $S_i^z \rightarrow -S_i^z$ by displaying long-range alternating magnetic order with a finite sublattice magnetization m^z at zero temperature. We assume m^z to be positive for simplicity, but its negative value is physically equivalent. At the spin isotropic point $\lambda = 1$ the continuous SU(2) symmetry is restored in the Heisenberg model so that the elementary excitations, the magnons, become Goldstone bosons with vanishing spin gap $\Delta = 0$ [6]. For any value $0 \leq \lambda < 1$ a finite energy gap $\Delta > 0$ is present, which takes the value $2J$ in the Ising limit $\lambda = 0$. No rigorously exact results are known for this model for $\lambda > 0$. But there is a wealth of evidence for its characteristic behavior [5,6,20]. Since the singular behavior at the Heisenberg point originates from Goldstone excitations and not by critical fluctuations, the associated exponents are expected to correspond exactly to the spin-wave values [21]. This has been confirmed by high order series expansions about the Ising limit as well as CST for the closing of the one-magnon gap Δ [10,21,22] with an exponent $1/2$.

B. Methods

Next, we briefly sketch the two approaches used.

1. Quantum Monte Carlo simulations

The starting point of the SSE QMC method is a high-temperature expansion of the quantum partition function:

$$Z = \text{Tr} e^{-\beta H} = \sum_{\{|\alpha\rangle\}} \sum_{n=0}^{\infty} \frac{\beta^n}{n!} \langle \alpha | (-H)^n | \alpha \rangle. \quad (2)$$

Here, $\{|\alpha\rangle\}$ denotes an orthonormal basis of the full Hilbert space and n the expansion order of the exponential term. Further, H is decomposed into a sum of local bond operators $H = -\sum_{b,t} H_{b,t}$, characterized by a bond b and an operator type t . These bond operators are chosen such that, given the basis $\{|\alpha\rangle\}$, they are nonbranching, i.e., $H_{b,t}|\alpha\rangle \propto |\alpha'\rangle$, $\forall |\alpha\rangle, |\alpha'\rangle \in \{|\alpha\rangle\}$. The standard approach for the basis, which we also use here, is a product state of local $|S_i^z\rangle$ eigenstates, i.e., $|\alpha\rangle = \bigotimes_{i=1}^N |S_i^z\rangle$, where N is the number of lattice sites. Here, a suitable bond decomposition is given by the operators

$$H_{b,1} = -J S_i^z S_j^z, \quad (3)$$

that are diagonal in $|\alpha\rangle$ as well as the off-diagonal bond operators

$$H_{b,2} = -\frac{J\lambda}{2} (S_i^+ S_j^- + S_i^- S_j^+). \quad (4)$$

The different products of bond operators contributing to Z can be encoded into an ordered operator sequence $S_n = [(t_1, b_1), \dots, (t_n, b_n)]$, thus yielding for the quantum partition function

$$Z = \sum_{\{|\alpha\rangle\}} \sum_{n=0}^{\infty} \sum_{\{S_n\}} \frac{\beta^n}{n!} \langle \alpha | H_{b_n, t_n} \cdots H_{b_2, t_2} H_{b_1, t_1} | \alpha \rangle. \quad (5)$$

The length of S_n corresponds to the expansion order and thus fluctuates. For numerical simulations, however, it is more convenient to truncate the sum to a maximal expansion order M . Since the average expansion order is (sharply) centered around $\langle n \rangle \propto N\beta$, this cutoff does not introduce any systematic error in practice as long as we always ensure $M \gg \langle n \rangle$. A fixed length operator string S_M can be obtained by padding S_n with unity operators $H_{0,0}$, which finally yields for the quantum partition function

$$Z = \sum_{\{|\alpha\rangle, S_M\}} \frac{\beta^n (M-n)!}{M!} \langle \alpha | \prod_{p=1}^M H_{b_p, t_p} | \alpha \rangle, \quad (6)$$

where an additional combinatorial factor $\binom{M}{n}^{-1}$ has to be introduced to account for the possible insertion positions of the unity operators. Here, the expansion order n corresponds to the number of nonunity operators in S_M . For a bipartite lattice, such as the square lattice considered here, all finite contributions to Z in Eq. (6) can be rendered positive, upon adding an appropriate constant C to the diagonal $H_{b,1} \rightarrow H_{b,1} + C$ [16]. To efficiently sample the configuration space $\{|\alpha\rangle, S_M\}$ by means of Markov chain Monte Carlo, a tandem of two updates is usually carried out. In a first local update step [16,17], diagonal operators are inserted or removed in S_M , effectively sampling the expansion order n . The next update is the directed-loop update [18,19]. Here, by carrying out a succession of local bond operator updates, a global and efficient update to sample different operator types, i.e., both

diagonal and off-diagonal, in S_M as well as $|\alpha\rangle$ is obtained. For more details we refer the reader to Refs. [18,23].

When approaching the Ising limit $\lambda \rightarrow 0$, we would ideally like our updating procedure to reduce to a classical (cluster) update on the spins in $|\alpha\rangle$. While this is indeed the case for the word-line based loop algorithm (see Ref. [24] for a review), which reduces in the Ising limit to a classical Swendsen-Wang cluster update [25] for $\beta \rightarrow \infty$ [26], this is not the case for the directed-loop update in the SSE picture for the following reasons. Flipping a spin in $|\alpha\rangle$ here corresponds to flipping the spin on all operators in S_M that are connected to that site. For the local bond operator updates during the directed-loop update, there is in the general case $\lambda \neq 1$ always the possibility to backtrack the loop propagation (this is also referred to as a ‘‘bounce’’). As the probability for these bounces becomes large for $\lambda \rightarrow 0$, this process becomes very inefficient for $\beta \rightarrow \infty$, since the number of operators connected to a site is proportional to β [18]. A simple trick to overcome this issue is to perform a unitary rotation in spin space, resulting in the Hamiltonian

$$\tilde{H} = J \sum_{\langle i,j \rangle} [S_i^x S_j^x + \lambda(S_i^y S_j^y + S_i^z S_j^z)]. \quad (7)$$

Rotating the Hamiltonian in spin space such that the largest matrix elements are associated with off-diagonal bond operators more generally seems to help with sampling issues that arise in the directed-loop update, as recently reported in spin-1 systems with single-ion anisotropies [27] or in spin-1/2 JQ_2 models [28].

Thus, we typically carry out simulations for the rotated Hamiltonian \tilde{H} . In the following, we briefly discuss how we measure the relevant observables, where $\langle \cdot \rangle_H$ ($\langle \cdot \rangle_{\tilde{H}}$) refers to thermal expectations with respect to H (\tilde{H}). We further note that we always simulate quadratic lattice geometries with $N = L^2$ sites and periodic boundary conditions.

In terms of the SSE, the energy is related to the average expansion order and given by $E = -\langle n \rangle_H / \beta = -\langle n \rangle_{\tilde{H}} / \beta$. To obtain an estimate of the ground-state energy e_0 per spin in the thermodynamic limit (TDL), we simulate E/N for linear system lengths $L = \{48, 64, 72\}$ at inverse temperature $\beta = L$ and linearly extrapolate the data, using the leading finite-size behavior L^{-3} .

While the spectrum of the Hamiltonian is not directly accessible within the SSE approach, it is indirectly encoded in imaginary time correlation functions

$$C(\tau) = \langle \hat{O}(\tau) \hat{O} \rangle = \langle e^{\tau H} \hat{O} e^{-\tau H} \hat{O} \rangle, \quad (8)$$

where \hat{O} is some operator and $\tau \in [0, \beta]$ denotes the imaginary time. If \hat{O} is chosen such that it excites the ground state, i.e., $\langle \text{GS} | \hat{O} | \text{GS} \rangle = 0$ and $\hat{O} | \text{GS} \rangle \neq 0$, the ground-state excitation gap Δ can be efficiently estimated in the TDL based on a (convergent) sequence of moments of $C(\tau)$ as introduced in Ref. [29]. Here an order m gap estimator $\Delta_{m,\beta}$ is constructed using the Fourier components of $C(\tau)$:

$$\tilde{C}(\omega_k) = \int_0^\beta C(\tau) e^{i\tau \omega_k} d\tau, \quad (9)$$

where $\omega_k = 2\pi k / \beta$, $k \in \mathbb{Z}$ denote bosonic Matsubara frequencies. The gap estimator $\Delta_{m,\beta}$ is then given as

follows:

$$\Delta_{m,\beta} = \omega_1 \sqrt{-\sum_{k=0}^m k^2 x_{m,k} \tilde{C}(\omega_k) / \sum_{k=0}^m x_{m,k} \tilde{C}(\omega_k)}, \quad (10)$$

where the numbers $x_{m,k}$ are defined by $x_{m,k} = 1 / \prod_{j=0, j \neq k}^m (k+j)(k-j)$. Here, the important property

$$\lim_{m \rightarrow \infty} \lim_{\beta \rightarrow \infty} \Delta_{m,\beta} = \lim_{\beta \rightarrow \infty} \lim_{m \rightarrow \infty} \Delta_{m,\beta} = \Delta \quad (11)$$

holds, where the limits are in particular interchangeable. For more details we refer the reader to Ref. [29]. A suitable operator for the one-magnon excitations is the staggered magnetization in the spin- x direction \hat{M}^x such that we consider $C(\tau) = \langle \hat{M}^x(\tau) \hat{M}^x \rangle_H = \langle \hat{M}^z(\tau) \hat{M}^z \rangle_{\tilde{H}}$. For the gap estimator $\Delta_{m,\beta}$, we measure $\tilde{C}(\omega_k)$ with respect to the rotated system \tilde{H} . In practice, as outlined in Ref. [29], a sufficient choice for convergence of $\Delta_{m,\beta}$ is given by $m = 5$ and $\beta = 2\pi / \tilde{\Delta}$, where $\tilde{\Delta}$ is an initial guess of Δ , for which we use the CST results. To eliminate finite-size effects, we choose linear system lengths of $L \approx 2\beta$, including system lengths up to $L = 384$ near the isotropic Heisenberg point.

The staggered longitudinal magnetization m^z can be obtained as $m^z = \sqrt{\langle (\hat{M}^z / N)^2 \rangle_H} = \sqrt{\langle (\hat{M}^x / N)^2 \rangle_{\tilde{H}}}$ from the spin-spin correlation function at maximal distance $\vec{r}_{\max} = (L/2, L/2)$ [20,23,30]:

$$\langle (\hat{M}^x / N)^2 \rangle_{\tilde{H}} = \begin{cases} \langle S_i^x S_j^x \rangle_{\tilde{H}}(r_{ij} = |\vec{r}_{\max}|), & \text{if } \lambda < 1 \\ 3 \langle S_i^x S_j^x \rangle_{\tilde{H}}(r_{ij} = |\vec{r}_{\max}|), & \text{if } \lambda = 1 \end{cases}, \quad (12)$$

where $r_{ij} = |\vec{r}_i - \vec{r}_j|$ and the factor 3 is included for $\lambda = 1$ to account for the SU(2) symmetry. The off-diagonal spin-spin correlation function $\langle S_i^x S_j^x \rangle_{\tilde{H}}$ can be efficiently measured during the directed-loop update [19,31]. To obtain an estimate of the ground-state magnetization m^z , we extrapolate data for linear system sizes $L = \{48, 64, 72\}$ at inverse temperatures $\beta = L$ to the TDL using the leading finite-size scaling behavior L^{-1} (here it is important to take the square root after the extrapolation). Close to the isotropic Heisenberg point, the finite-size effects are stronger, and we here linearly extrapolate data for linear system sizes $L = \{96, 128, 140, 160\}$ at inverse temperatures $\beta = L$.

The transverse correlation length ξ^x quantifies the exponential asymptotic decay of the spin-spin correlation function $\langle S_i^x S_j^x \rangle_H \propto \exp(-r_{ij} / \xi^x) / r_{ij}$. It is always finite for $\lambda < 1$ and relates to the quantum fluctuations that arise for $\lambda \neq 0$. In addition to the dominant exponential term an algebraic factor $1/r_{ij}$ appears for the two-dimensional system considered here. In Appendix A, we provide a general derivation of the algebraic correction factor within a saddle point approximation for general dimensions, and identify its actual presence explicitly for the system under consideration from QMC simulations in Sec. III. One possible means of extracting the correlation length ξ^x is thus to perform a fit of the numerical data to this asymptotic decay within appropriate ranges of the distance r_{ij} . Another standard approach to estimate ξ^x is by means of the staggered spin structure factor $S^x(\vec{q})$,

defined by

$$\begin{aligned} S^x(\vec{q}) &= \frac{1}{N} \sum_{i,j} (\pm 1) e^{-i\vec{q}\cdot(\vec{r}_i - \vec{r}_j)} \langle S_i^x S_j^x \rangle_H \\ &= \frac{1}{N} \sum_{i,j} (\pm 1) e^{-i\vec{q}\cdot(\vec{r}_i - \vec{r}_j)} \langle S_i^z S_j^z \rangle_{\tilde{H}}, \end{aligned} \quad (13)$$

where for the staggering sign “+1” is chosen if the sites i and j belong to the same sublattice and “−1” otherwise. In terms of this quantity, ξ^x can be estimated by the second-moment estimator

$$\xi^x = \sqrt{2} \frac{1}{|\vec{q}_1|} \sqrt{\frac{S^x(\vec{0})}{S^x(\vec{q}_1)} - 1}, \quad (14)$$

where $\vec{q} = \vec{0}$ corresponds to the antiferromagnetic ordering and $\vec{q}_1 = \vec{e}_x 2\pi/L$ is one of the reciprocal lattice vectors closest to $\vec{0}$. The factor $\sqrt{2}$ is specific to the algebraic correction term $1/r_{ij}$ in the spin-spin correlation function (see Appendix B for other cases). For our analysis, we focus on the regime $\lambda \geq 0.8$. The measurement of off-diagonal correlation functions during the directed-loop update is known to yield better statistics compared to measuring diagonal correlation functions [19,31]. Since for the regime $\lambda \geq 0.8$ efficient simulations can be carried out without performing a spin rotation, we thus measure $\langle S_i^x S_j^x \rangle_H$ as an off-diagonal observable during the directed-loop update. Further, we extrapolate the data to the TDL using polynomials of degree 3 in $1/L$ for linear system sizes up to $L = 100$ and at inverse temperature $\beta = 1/L$.

2. Continuous similarity transformations

For the semianalytic CST approach we rewrite the spin model (1) in terms of bosons according to Dyson and Maleev [32,33] which hides the manifest Hermiticity of the Hamiltonian. But it ensures that the bosonic Hamiltonian

$$\begin{aligned} H = J \sum_{i \in \Gamma_{A,\delta}} \left[-S^2 + S(a_i^\dagger a_i + b_{i+\delta}^\dagger b_{i+\delta}) \right. \\ \left. + \lambda a_i b_{i+\delta} + \lambda a_i^\dagger b_{i+\delta}^\dagger \right. \\ \left. - a_i^\dagger a_i b_{i+\delta}^\dagger b_{i+\delta} - \frac{\lambda}{2} a_i^\dagger a_i b_{i+\delta} - \frac{\lambda}{2} a_i^\dagger b_{i+\delta}^\dagger b_{i+\delta} b_{i+\delta} \right] \end{aligned} \quad (15)$$

comprises at maximum quartic terms in the bosonic creation and annihilation operators. Here the sum runs over the sites of the A sublattice Γ_A where the a bosons are located. The b bosons are located on the B sublattice Γ_B while the δ links nearest neighbors, i.e., a site on Γ_A to one of its adjacent sites on Γ_B .

The next step is to Fourier transform the bosonic operators to $a_{\mathbf{k}}$ and $b_{\mathbf{k}}$ and their Hermitian conjugates, which yields the Hamilton operator with bilinear and quartic bosonic terms in reciprocal space with wave vectors \mathbf{k} . These wave vectors are chosen from the magnetic Brillouin zone because we distinguish between both sublattices. Subsequently, we perform a standard Bogoliubov transformation to operators $\alpha_{\mathbf{k}}$ and $\beta_{\mathbf{k}}$ to eliminate the bilinear terms creating or annihilating pairs of bosons. This is done self-consistently, i.e., the bilinear terms

changing the number of bosons vanish after normal ordering all quartic terms. Normal ordering is meant here relative to the bosonic vacuum after the Bogoliubov transformation: all creation operators are commuted to the left, and all annihilation operators are commuted to the right. Truncating the resulting Hamiltonian at the bilinear level provides the usual mean-field Hamiltonian which neglects all interactions between the elementary excitations, but comprises a static renormalization of the dispersion on the level of a self-consistent Hartree-Fock theory.

We proceed by keeping all quartic terms, which generally consist of three classes of terms: (i) leaving the number of bosons invariant, (ii) changing this number by ± 2 , and (iii) changing this number by ± 4 . Class (i) consists of terms with two creation and two annihilation operators, and class (ii) consists of terms with three creation and one annihilation operator or vice versa. Finally, class (iii) consists of terms with four creation operators or four annihilation operators.

This quartic Hamiltonian is not manifestly Hermitian because of the properties of the Dyson-Maleev representation. Thus, we apply a CST to it which is not manifestly unitary. The flow of coupling constants results from

$$\frac{d}{d\ell} H(\ell) = [\eta(\ell), H(\ell)], \quad (16)$$

where ℓ is the continuous flow parameter running from $\ell = 0$ where H equals the initial Hamiltonian to $\ell = \infty$ where one obtains an effective Hamiltonian $H_{\text{eff}} = H(\infty)$ [34,35]. The initial Hamiltonian results from the self-consistently determined Bogoliubov transformation while the final effective Hamiltonian H_{eff} no longer contains terms of classes (ii) and (iii). In order to reach this nice property, which facilitates the subsequent interpretation, we choose the particle conserving generator $\eta_{\text{PC}}(\ell)$ [36,37] which includes all terms in the Hamiltonian at ℓ of classes (ii) and (iii). Those terms which increase the number of bosons have exactly the same prefactor as in $H(\ell)$ while those terms which decrease the number of bosons have the opposite sign in the prefactor of the same term in $H(\ell)$.

Assuming convergence of the flow implies $\eta(\infty) = 0$ so that H_{eff} conserves the number of excitations, here magnons. Then, the energy of single-magnon states can be read off directly from the dispersion $\omega(\mathbf{k})$ without any further many-body corrections. In order to be able to solve (16) two further approximations are necessary. First, we solve the problem for a finite cluster of L^2 sites for various boundary conditions so that there is a finite number of points in reciprocal space. We point out that, compared to QMC, a unit cell with two sites is chosen with L^2 points for each sublattice Γ_A and Γ_B resulting in a total of $N = 2L^2$ points. Second, on the right hand side of (16) quartic terms are also commuted with quartic terms so that hexatic terms are generated. First, we normal order them so that their constant, bilinear, and quartic content is kept. But the genuine hexatic terms are not included because of their higher scaling dimension [7,9,10]. This introduces a small truncation error for intermediate anisotropies. But close to the isotropic point $\lambda = 1$ we hardly detect truncation errors [10].

The constant arising in H_{eff} is the ground-state energy E_0 . The total sublattice magnetization M^z in z direction can be

found as the derivative of the ground-state energy with respect to an alternating magnetic field h_{alt} :

$$M^z = \frac{d}{dh_{\text{alt}}} E_0 \Big|_{h_{\text{alt}}=0} \quad (17)$$

according to the Hellmann-Feynman theorem. In practice, we compute the derivative by the ratio $[E_0(h_{\text{alt}}) - E_0(0)]/h_{\text{alt}}$ for small $h_{\text{alt}} \approx 10^{-7}J$.

The ground-state energy per site and the sublattice magnetization per site are denoted e_0 and m^z , respectively. The magnon dispersion is denoted $\omega(\mathbf{k})$; its minimum defines the spin gap Δ which is located at $\vec{k} = (\pi, \pi)$. The correlation length is computed based on the full dispersion choosing a direction $\mathbf{n} = \mathbf{e}_x$ in reciprocal space, first fitting the squared dispersion by a sum of cosine terms

$$\omega(k)^2 = \sum_{n=0}^{L/2} A_n \cos(nk) \quad (18)$$

(see Ref. [38] and Appendix A) and then solving

$$\omega(i\kappa \mathbf{n}) = 0 \quad \text{with } \text{Re } \kappa = 1/\xi \quad (19)$$

according to a generalization of the results in Ref. [38] from one to two dimensions (see Appendix A for the generalization to any spatial dimension including also leading power law corrections). In the dispersions studied here, we never found a value of κ with a finite imaginary part. Finally, the results obtained for L^2 sites for various boundary conditions are extrapolated to the thermodynamic limit $L \rightarrow \infty$. We use results for $L \in \{17, 19, 21\}$ and antiperiodic boundary conditions because odd linear lengths and these boundary conditions display the smallest dependence on the finite size of the evaluated cluster. For the technical details, we refer to Refs. [7,9,10].

III. RESULTS

The key results of the ground-state properties of the anisotropic spin-1/2 XXZ antiferromagnet on the square lattice are collected in Fig. 1. The CST data for the ground-state energy, spin gap, and the correlation length have been published in Ref. [10] already. Overall, the QMC and CST data agree extremely well.

In the ground-state energy per site e_0 , the relative errors of the QMC data are of order 10^{-6} . The systematic error of the finite-size extrapolation is negligible, i.e., much smaller than the statistical errors. The error of the CST data is systematic since no stochastic aspects are involved. Two main error sources can be identified: (i) the truncation of the flowing Hamiltonian to quartic order and (ii) the finite-size effect. The finite-size effect can be assessed by varying the extrapolations and the boundary conditions, and we estimate it to be of order 10^{-5} . The effect of the truncation cannot be estimated intrinsically, but only by comparison to results from other methods. We find that above $\lambda \approx 0.4$ the CST data start to deviate from the QMC data. This deviation appears to be systematic, since it does not change in sign and furthermore evolves smoothly. The deviation becomes maximum around $\lambda \approx 0.9$, where it is approximately 2×10^{-4} . We analyze the deviations of the

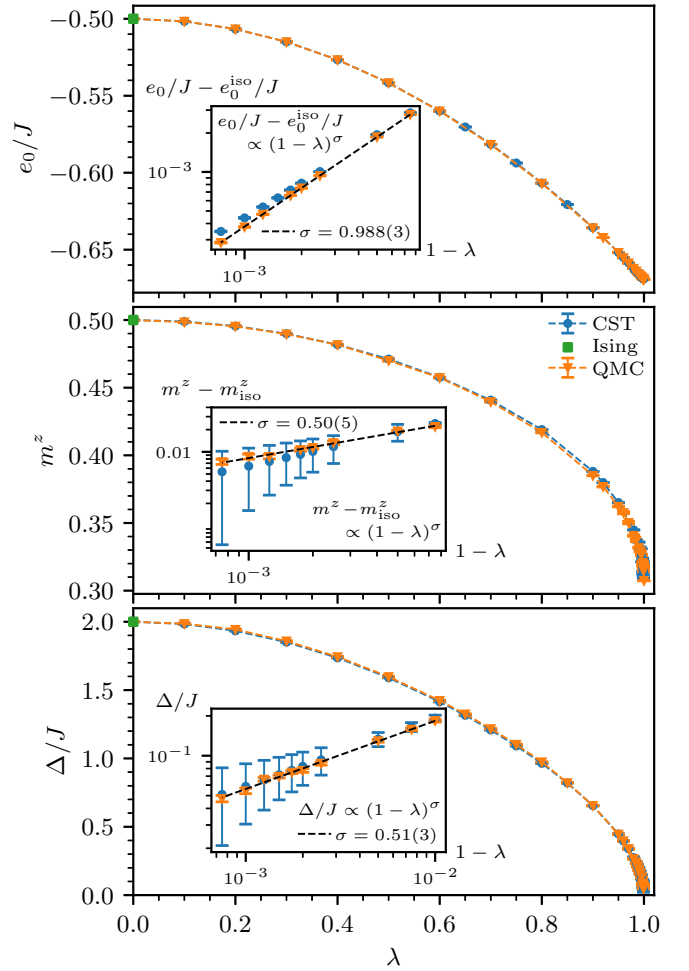


FIG. 1. Comparison of ground-state data obtained by CST (circles) and QMC (triangles) both extrapolated to the TDL. The points at $\lambda = 0$ (green marker) denote the exact result of the 2D Ising model. All QMC errors are statistical and smaller than the marker size. Upper panel: Ground-state energy per site e_0 . The relative statistical QMC errors are of order 10^{-6} . The systematic error of the CST data is estimated to be of order 10^{-5} . The inset shows that the energy approaches its isotropic value linearly agreeing with previous results [39,40]. Middle panel: Sublattice magnetization per site m^z . The relative statistical QMC errors are of order 10^{-3} ; the CST error is of order 10^{-4} . In addition, we presume that the CST has a small systematic error. The inset shows that the sublattice magnetization approaches its isotropic value like a square root agreeing with mean-field results [39,40]. Lower panel: Spin gap Δ with errors shown in the inset. The data provide strong evidence for $\Delta \propto \sqrt{1-\lambda}$ as assumed previously [39,40].

CST results from the QMC results in Appendix C including a detailed comparison. Still the agreement is very good.

Repeating the estimates for the sublattice magnetization per site m^z , we arrive at relative statistical QMC errors of order 10^{-3} . In terms of the CST, the error of the finite-size effect and the effect of approximating a derivative by a ratio in the CST data is estimated as 10^{-4} . The deviation between the data from QMC and CST becomes here maximal around $\lambda \approx 0.9$ as well, where it is around 5×10^{-3} in absolute terms corresponding to $\approx 1.3\%$. This deviation, similarly to

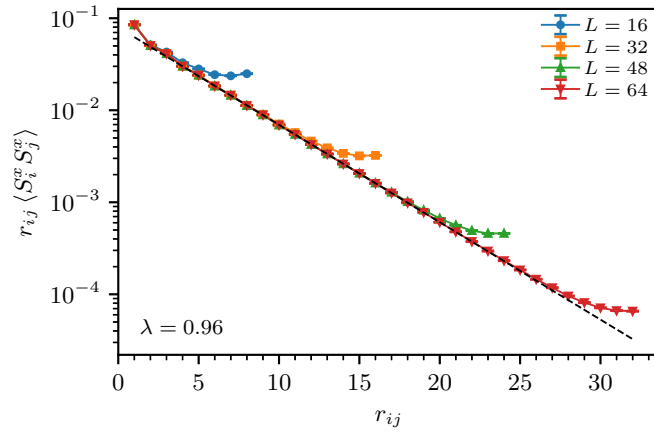


FIG. 2. Rescaled transverse spin-spin correlations $r_{ij} \langle S_i^x S_j^x \rangle$, obtained from QMC simulations at $\lambda = 0.96$, as functions of the distance r_{ij} for systems of different linear system sizes L , plotted in logarithmic form in order to probe the approach towards the anticipated asymptotic behavior. The black dashed line depicts the excellent agreement with the exponential behavior $r_{ij} \langle S_i^x S_j^x \rangle \propto \exp(-r_{ij}/\xi^x)$.

the deviation observed for the energy, does not change sign and evolves relatively smoothly. Thus, we presume that it is systematic and can be attributed to the CST truncation. Still, the agreement of the data from the two distinct approaches over the whole parameter range is very good.

Next, we address the value of the spin gap Δ . The relative statistical errors of the QMC data are of order 10^{-3} and near the isotropic Heisenberg point of order 10^{-2} . The relative error estimate for the CST data yields 10^{-4} and lower for $\lambda < 0.9$ and rises up to 0.66% close to the isotropic point. While there is a small systematic deviation of the CST data, both approaches agree very well. We highlight that the double-logarithmic plot in the inset of the lowest panel in Fig. 1 displays an excellent agreement. Both data sets support the conclusion that the spin gap vanishes in a square-root fashion $\propto \sqrt{1-\lambda}$, as reported in Refs. [39,40]. Similarly, the magnetization approaches its value for the isotropic Heisenberg model also following a square-root law.

Finally, we consider the correlation length ξ . Since we are dealing with a long-range ordered phase at all values of λ in the ground state of the Hamiltonian (1) this leads to an infinite (longitudinal) correlation length in the S^z direction. But the magnons stand for transversal fluctuations of this order parameter. Hence, we consider the transversal correlation length ξ^x pertaining to the dominantly exponential decay of $\langle S_i^x S_j^x \rangle \propto \exp(-r_{ij}/\xi^x)/r_{ij}$ for large values of r_{ij} .

As shown in Appendix A for this two-dimensional system, an additional algebraic factor $1/r_{ij}$ appears in the asymptotic scaling. We can demonstrate the above scaling behavior also based on QMC simulations. This is illustrated for the case of $\lambda = 0.96$ in Fig. 2. As we consider systems with periodic boundary conditions, the correlations $\langle S_i^x S_j^x \rangle$ for a system size L are shown for distances $r_{ij} \leq L/2$. We find that the rescaled quantity $r_{ij} \langle S_i^x S_j^x \rangle$ approaches an exponential decay, as anticipated. By fitting the rescaled QMC data for $L = 64$ to an exponential decay (see solid black line in Fig. 3), within the regime of r_{ij} between 5 and 20, we thus obtain a robust

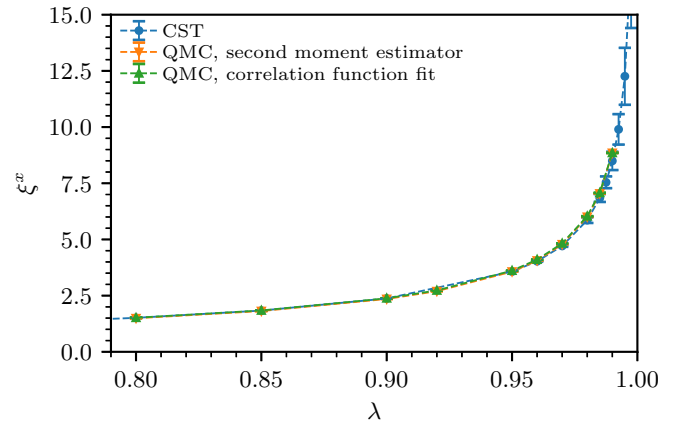


FIG. 3. Ground-state transverse correlation length ξ^x as a function of λ in the infinite-size limit obtained by CST (circles) and QMC (triangles).

estimate for the correlation length ξ^x in the TDL. We also used the improved second-moment estimator in Eq. (14) in order to obtain the correlation length ξ^x from the structure factor which is extrapolated to the TDL including systems up to $L = 100$ with $\beta = L$. In CST, as given in Eq. (18), we describe the square of the dispersion $\omega(\mathbf{k})$ obtained numerically by a sum of cosine terms such that the dispersion is exactly captured. Then, we determine the correlation length by solving for the zeros in (19). Again, as shown in Fig. 3, the agreement is very good.

Concerning the power laws upon approaching the isotropic Heisenberg point, the CST and the QMC data sets strongly support the linear behavior of the ground-energy and square-root behavior for the sublattice magnetization, the spin gap, and the correlation length. The latter two power laws are not independent, but linked according to $\xi \propto 1/\Delta$. All these power laws agree with the results of spin-wave theory [39] which may appear surprising. But we emphasize that approaching the isotropic point does not represent a true quantum phase transition because the system stays in the same long-range ordered phase. The observed gap closure does not indicate a second order transition, but the restoration of the continuous symmetry of spin rotation which in turn implies the occurrence of Goldstone bosons. Since no critical quantum fluctuations appear the exponents remain the same as in mean-field theory. Our findings are further in agreement with very recent density-matrix renormalization-group studies [41].

IV. CONCLUSIONS

In this paper we examined the ground-state properties of the anisotropic spin-1/2 XXZ quantum antiferromagnet on the two-dimensional square lattice in the thermodynamic limit. For this purpose we considered two approaches, namely unbiased SSE QMC simulations as well as the semianalytic CST method.

Based on our analysis of the ground-state energy e_0 , the excitation gap Δ , the sublattice magnetization m^z , as well as the transverse correlation length ξ^x , we report a very good agreement of both approaches over the whole parameter range, from the Ising limit $\lambda = 0$ to the SU(2) symmetric isotropic

Heisenberg point $\lambda = 1$. Our findings support the quantitative validity of both approaches. In terms of the CST approach, this is particularly interesting as the method may be applied to extract quantum-critical properties as well as dynamical correlation functions of frustrated systems such as the J_1 - J_2 model or the Heisenberg model on the triangular lattice, where the statistical accuracy of QMC methods is severely limited, due to the sign problem.

Our data are available in Ref. [42] and provide quantitative reference results in the thermodynamic limit; the raw data are available upon request. We envision this to be of particular use for benchmarking purposes of numerical approaches for strongly correlated quantum spin systems.

ACKNOWLEDGMENTS

This work has been financially supported by the Deutsche Forschungsgemeinschaft (DFG, German Research Foundation) in Projects No. UH 90/14-1 (D.-B.H. and G.S.U.), No. SCHM 2511/13-1 (M.R.W. and K.P.S.), and No. RTG 1995 (N.C. and S.W.). N.C. further acknowledges support by the Agence nationale de la recherche (ANR, French National Research Agency) through grant LODIS (No. ANR-21-CE30-0033) and thanks the IT Center at RWTH Aachen University for access to computing time. K.P.S. gratefully acknowledges support by DFG Project No. 429529648-TRR 306 QuCoLiMa (“Quantum Cooperativity of Light and Matter”) and the Munich Quantum Valley, which is supported by the Bavarian state government with funds from the Hightech Agenda Bayern Plus. M.R.W. and K.P.S. thankfully acknowledge the scientific support and high-performance computing resources provided by the Erlangen National High Performance Computing Center (NHR@FAU) of the Friedrich-Alexander-Universität Erlangen-Nürnberg.

APPENDIX A: CORRELATION FUNCTION FROM THE ONE-PARTICLE DISPERSION

This Appendix contains a generalization of the results of Ref. [38] from one to any spatial dimension concerning the computation of the correlation length based on the full one-particle dispersion. In addition, we also derive the leading power law corrections.

We consider a translationally invariant system on a lattice in which the elementary excitations are bosonic and display a gap. Note that an ordered antiferromagnet on a bipartite lattice can be made translationally invariant by a 180° rotation of the spins on one sublattice so that it belongs to the considered kind of systems. The Hamiltonian reads

$$H = \sum_{\vec{k} \in \text{BZ}} \left[A_{\vec{k}} b_{\vec{k}}^\dagger b_{\vec{k}} + \frac{1}{2} B_{\vec{k}} (b_{\vec{k}}^\dagger b_{-\vec{k}}^\dagger + b_{\vec{k}} b_{-\vec{k}}) \right] + H_1, \quad (\text{A1})$$

where $b_{\vec{k}}^{(\dagger)}$ are the usual bosonic annihilation (creation) operators and H_1 is an interaction term which does not need to be specified further. The lattice constant is henceforth set to unity. Neglecting the interaction, the dispersion reads

$$\omega_{\vec{k}}^2 = A_{\vec{k}}^2 - B_{\vec{k}}^2 > 0 \quad (\text{A2})$$

and the correlation $G_{\vec{r}} := \langle b_j^\dagger b_i \rangle$ with $\vec{r} := \vec{r}_j - \vec{r}_i$ is given at zero temperature by

$$G_{\vec{r}} = \frac{1}{(2\pi)^d} \int_{\text{BZ}} \langle b_{\vec{k}}^\dagger b_{\vec{k}} \rangle \exp(i\vec{r} \cdot \vec{k}) d\vec{k}^d \quad (\text{A3a})$$

$$= \frac{1}{2(2\pi)^d} \int_{\text{BZ}} \left(\frac{A_{\vec{k}}}{\omega_{\vec{k}}} - 1 \right) \exp(i\vec{r} \cdot \vec{k}) d\vec{k}^d. \quad (\text{A3b})$$

If we include interaction effects, the functions $A_{\vec{k}}$ and $B_{\vec{k}}$ will be modified and hence $\omega_{\vec{k}}$. For simplicity, we refrain from introducing new labels for these modified quantities. In addition, Eq. (A3b) does not hold anymore in a rigorous sense because of multiboson contribution. But multiboson contributions form continua in the (ω, \vec{k}) space which induce dependences in real space which decay quicker than the contributions of the δ distributions resulting from the single-boson states. However, the weights of the single-boson states are reduced due to hybridization with multiboson states. Introducing a weight factor $Z_{\vec{k}}$ yields for the long-range part $G_{\vec{r}}^{\text{LR}}$ of the correlation

$$G_{\vec{r}}^{\text{LR}} = \frac{1}{2(2\pi)^d} \int_{\text{BZ}} Z_{\vec{k}} \frac{A_{\vec{k}}}{\omega_{\vec{k}}} \exp(i\vec{r} \cdot \vec{k}) d\vec{k}^d \quad (\text{A4})$$

where we also left out the constant background stemming from the summand -1 in (A3b).

From (A4) one realizes that a significant contribution results from small values of the dispersion. But this observation is not yet sufficient to find the correlation length. For this, the saddle point approximation needs to be invoked. For clarity, we first discuss the one-dimensional case (see Ref. [38]).

1. One dimension

The dispersion can be described by a sum of trigonometric functions so that it is analytic. Note that the finite gap $0 < \Delta \leq \omega_k$ avoids the occurrence of singularities. The same holds true for the numerator $Z_k A_k$. Then we can shift the integration from the real axis to a path γ in the complex plane crossing a point where $\omega_{k_0} = 0$:

$$G_x^{\text{LR}} = \frac{1}{4\pi} \int_{\gamma} Z_k \frac{A_k}{\omega_k} \exp(ikx) dk. \quad (\text{A5})$$

In order to deal with the singularity in the above integrand, we substitute k by $k(z)$ fulfilling

$$\frac{dk}{dz} = \omega_k \Leftrightarrow \frac{dz}{dk} = 1/\omega_k. \quad (\text{A6})$$

We denote by z_0 the point in \mathbb{C} with $k(z_0) = k_0$. The chain rule implies

$$k'' = \frac{d^2 k}{dz^2} = \frac{d\omega_k}{dk} \frac{dk}{dz} = \frac{d\omega_k}{dk} \omega_k = \frac{1}{2} \frac{d(\omega_k^2)}{dk}. \quad (\text{A7})$$

By $\tilde{\gamma}$ we denote the contour of which the image is the original contour, i.e., $\gamma = k(\tilde{\gamma})$ with $k(z_1) = -\pi$ and $k(z_2) = \pi$. Then we can write

$$G_x^{\text{LR}} = \frac{1}{4\pi} \int_{\tilde{\gamma}} Z(z) A(z) \exp[ixk(z)] dz. \quad (\text{A8})$$

This integration can be evaluated for $x \rightarrow \infty$ by the saddle point approximation, also known as the method of the steepest

descent, yielding

$$G_x^{\text{LR}} = \frac{1}{4\pi} Z(z_0) A(z_0) \exp(ixk_0) \sqrt{\frac{2\pi}{x|k_0''|}}, \quad (\text{A9})$$

where $k_0'' := \frac{d^2k}{dz^2}|_{z=z_0}$. With $1/\xi = \text{Im}k_0$ we obtain

$$G_x^{\text{LR,1D}} \propto \frac{\exp(-|x|/\xi)}{\sqrt{|x|}}. \quad (\text{A10})$$

For $x \rightarrow -\infty$, we repeat the above reasoning for $-k_0$ which also fulfills $\omega_{-k_0} = 0$ if the dispersion is even as is the case for systems with inversion symmetry.

We stress that the above derivation yields the power law correction $1/\sqrt{|x|}$ in addition to the exponential decrease. Note that this power law differs from the classical Ornstein-Zernike law [43].

2. Two dimensions

In essence, we repeat the arguments of the one-dimensional case. But the integration over the wave vectors is two-dimensional. We solve this issue by assuming rotational invariance of the asymptotic behavior in space, i.e., only $r = |\vec{r}|$ matters. Correspondingly, we assume that the integrand in (A4) is rotationally invariant in reciprocal space. This is not completely true, but can be justified *a posteriori*: we found that ξ hardly depends on the direction $(1, 0)^\top$ or $(1, 1)^\top$. The difference is only a few percent in the range $\xi \approx 1$ and vanishes exponentially for larger correlation lengths.

Under the assumption of rotational invariance Eq. (A4) becomes

$$G_{\vec{r}}^{\text{LR}} \approx \frac{1}{8\pi^2} \int_0^\pi \int_0^{2\pi} k Z_k \frac{A_k}{\omega_k} \exp(irk \cos \varphi) d\varphi dk \quad (\text{A11a})$$

$$= \frac{1}{4\pi} \int_0^\pi k Z_k \frac{A_k}{\omega_k} J_0(rk) dk. \quad (\text{A11b})$$

The upper limit of the k integration is an approximation, but one does not need to bother because it does not enter the saddle point approximation. The function $J_\nu(z)$ is the ν th Bessel function of the first kind. Its asymptotic behavior for large arguments is

$$J_\nu(z) \propto \text{Re} \exp[iz - \pi(\nu + 1/2)/2]/\sqrt{z} \quad (\text{A12})$$

so that we can apply again the substitution and the saddle point approximation as in the one-dimensional case yielding finally

$$G_r^{\text{LR,2D}} \propto \frac{\exp(-r/\xi)}{r} \quad (\text{A13})$$

with $1/\xi = \text{Im}(k_0)$ from $\omega_{k_0} = 0$ as before. Note that the additional power law results from the asymptotic behavior of the Bessel function which in turn stems from the angular integration. It reflects how large the contribution of $\exp(irk)$ is.

3. Three dimensions

We repeat the arguments for the two-dimensional case. Assuming rotational invariance as in two dimensions the integration over the solid angle yields

$$\frac{1}{4\pi} \int_\Omega d\Omega \exp[irk \cos(\vartheta)] = \frac{1}{2} \int_{-1}^1 \exp(irku) du \quad (\text{A14a})$$

$$= \frac{1}{rk} \text{Im} \exp(irk). \quad (\text{A14b})$$

As to be expected, the exponential dependence remains the same, but the power law exponent is lowered by 1/2. This leads us to

$$G_r^{\text{LR,3D}} \propto \frac{\exp(-r/\xi)}{r^{3/2}} \quad (\text{A15})$$

with $1/\xi = \text{Im}(k_0)$ from $\omega_{k_0} = 0$ as before.

4. Arbitrary dimension

The obvious generalization of the above findings reads

$$G_r^{\text{LR,AD}} \propto \frac{\exp(-r/\xi)}{r^{d/2}} \quad (\text{A16})$$

in d dimensions with $1/\xi = \text{Im}(k_0)$ from $\omega_{k_0} = 0$. Note that $d - 1$ factors of \sqrt{r} in the denominator result from a phase space argument or geometrical dilution. But one factor \sqrt{r} stems from the saddle point approximation (see the derivation in one dimension).

Equation (A16) can be derived as before. First, we integrate in (A4) over all angles at fixed modulus q . We choose \vec{r} to point along \vec{e}_1 so that $\vec{r} \cdot \vec{k} = rk_1$ and the angular integration yields

$$f(r, q) = \int_{\text{BZ}} e^{i\vec{r} \cdot \vec{k}} \delta(k - q) dk^d \quad (\text{A17a})$$

$$= \int_{-q}^q e^{irk_1} \delta(k - q) dk_{\perp}^{d-1} dk_1 \quad (\text{A17b})$$

$$= \int_{-q}^q \int_0^q e^{irk_1} \delta(k - q) \rho_{d-1}(k_{\perp}) dk_{\perp} dk_1 \quad (\text{A17c})$$

where we denoted k for $\sqrt{k_1^2 + k_{\perp}^2}$ and used \vec{k}_{\perp} for the wave vector perpendicular to \vec{e}_1 and the density of the modulus k_{\perp} is given in dimension d by $\rho_d(k_{\perp}) \propto k_{\perp}^{d-1}$. The integration over k_{\perp} is carried out with the help of the δ distribution yielding

$$f(r, q) = q \int_{-q}^q e^{irk_1} \frac{\rho_{d-1}(\sqrt{q^2 - k_1^2})}{\sqrt{q^2 - k_1^2}} dk_1 \quad (\text{A18a})$$

$$\propto q \int_{-q}^q e^{irk_1} (q^2 - k_1^2)^{(d-3)/2} dk_1 \quad (\text{A18b})$$

$$= q^{d-1} \int_{-1}^1 e^{irqx} (1 - x^2)^{(d-3)/2} dx \quad (\text{A18c})$$

$$= q^{d/2} \sqrt{\pi} \left(\frac{2}{r}\right)^{d/2-1} \Gamma((d-1)/2) J_{d/2-1}(rq) \quad (\text{A18d})$$

where we substituted $k_1 = qx$. In the final integration over q , we use again the asymptotics (A12) and

employ the saddle point approximation to obtain (A16) stated above.

Equation (A16) constitutes the powerful generalization of the one-dimensional result in Ref. [38] to arbitrary dimension including the leading multiplicative power law corrections.

We finally note that the above result in Eq. (A16) results from replacing in the Ornstein-Zernike law for the correlation function [43] in d spatial dimensions, $G^{\text{OZ}}(r) \propto \exp(-r/\xi_x)/r^{(d-1)/2}$, the dimension d by $d+1$, corresponding to the usual quantum-to-classical mapping.

APPENDIX B: QMC ESTIMATOR FOR THE CORRELATION LENGTH

In this Appendix, we discuss the QMC estimator for the correlation length in different spatial dimensions and for different correlation function asymptotics. In the case of the Ornstein-Zernike form of the correlation function [43] in d spatial dimensions, $\langle S_i^x S_j^x \rangle \propto \exp(-r_{ij}/\xi^x)/r_{ij}^{(d-1)/2}$, the improved second-moment estimator reads

$$\xi^x = \sqrt{\frac{8d}{(1+d)(3+d)}} \frac{1}{|\vec{q}_1|} \sqrt{\frac{S^x(\vec{0})}{S^x(\vec{q}_1)} - 1}, \quad (\text{B1})$$

as discussed in Ref. [23] [note that there is an apparent typo in Eq. (71) of Ref. [23]]. The numerical prefactor in the above estimator is of order 1 and thus often ignored when extracting correlation lengths based on this estimator. Indeed, for $d=1$ and 3 the prefactor simplifies to 1 exactly, while for $d=2$ it reads $\sqrt{16/15}$, explicitly. For other algebraic factors in the correlation function asymptotics, the numerical prefactor however differs. In particular, for the asymptotic behavior $\langle S_i^x S_j^x \rangle \propto \exp(-r_{ij}/\xi^x)/r_{ij}^{d/2}$ derived in the preceding Appendix we similarly obtain, upon analytically performing the Fourier transformation in the continuum limit, the corresponding prefactors $\sqrt{8/3}$, $\sqrt{2}$, and $\sqrt{4/3}$ for $d=1, 2, 3$, respectively.

APPENDIX C: QUANTITATIVE COMPARISON OF CST AND QMC RESULTS

Here, we show a quantitative comparison of the CST and QMC results in terms of the statistical and systematic errors. In Fig. 4 the deviations of the CST data relative to the QMC data are plotted for the ground-state energy per site e_0 , the magnetization per site m^z , and the energy gap Δ . In energy and magnetization the deviation is remarkably small for small values of λ growing for large λ . We attribute this to the truncation of the tracked terms on quartic level corresponding to scaling dimension 2. Hence, it is a systematic deviation which we had observed before in the binding energies of two-magnon bound states [10]. We do not have a complete understanding of the deviations of the spin gap which is rather constant. Still, we presume a systematic origin linked to the truncation in the CST approach. Remarkably, the deviations decrease in all three quantities upon approaching the isotropic point. We interpret this as a justification of the truncation according to scaling dimension which allows us to find the

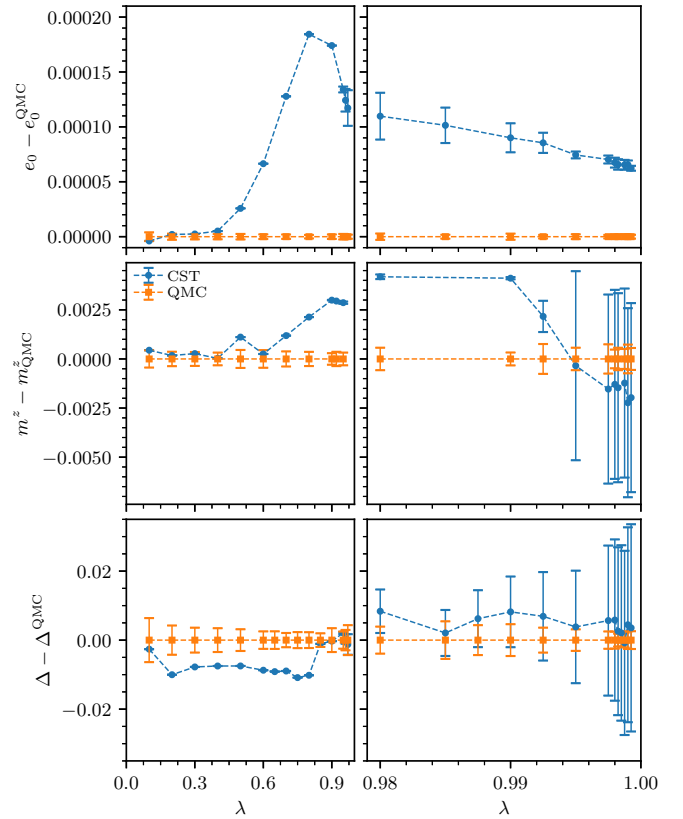


FIG. 4. Quantitative comparison of the CST and QMC results in the TDL of the ground-state energy e_0 (top panels), the ground-state magnetization m^z (middle panels), and the spin gap Δ (bottom panels) as a function of λ .

relevant effective model close to the isotropic point almost quantitatively.

Finally, Fig. 5 displays the deviation of three ways to access the transversal correlation length. The two QMC estimators agree well below the 1% level. Such minor deviations may result from uncertainties in performing the actual finite-size fitting process. The CST results acquire large errors

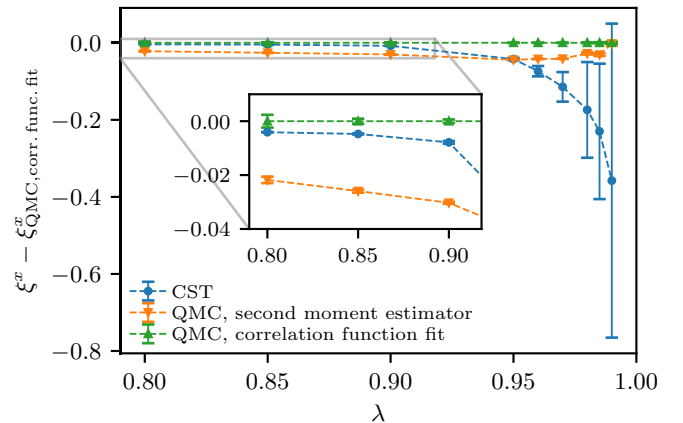


FIG. 5. Quantitative comparison of CST (circles) and QMC (triangles) results of the ground-state transverse correlation length ξ^x extrapolated to the thermodynamic limit as a function of λ .

close to the isotropic point because the correlation length depends inverse proportionally on the spin gap so that tiny

inaccuracies in the latter induce large inaccuracies in the correlation length.

-
- [1] C. Chappert, A. Fert, and F. Van Dau, The emergence of spin electronics in data storage, *Nat. Mater.* **6**, 813 (2007).
- [2] V. Baltz, A. Manchon, M. Tsoi, T. Moriyama, T. Ono, and Y. Tserkovnyak, Antiferromagnetic spintronics, *Rev. Mod. Phys.* **90**, 015005 (2018).
- [3] O. Gomonay, T. Jungwirth, and J. Sinova, Concepts of antiferromagnetic spintronics, *Phys. Status Solidi: Rapid Research Letters* **11**, 1700022 (2017).
- [4] J. G. Bednorz and K. A. Müller, Possible high- T_c superconductivity, *Z. Phys. B* **64**, 189 (1986).
- [5] E. Manousakis, The spin- $\frac{1}{2}$ Heisenberg antiferromagnet on a square lattice and its application to the cuprous oxides, *Rev. Mod. Phys.* **63**, 1 (1991).
- [6] A. Auerbach, *Interacting Electrons and Quantum Magnetism*, Graduate Texts in Contemporary Physics (Springer, New York, 1994).
- [7] M. Powalski, G. S. Uhrig, and K. P. Schmidt, Roton minimum as a fingerprint of magnon-Higgs scattering in ordered quantum antiferromagnets, *Phys. Rev. Lett.* **115**, 207202 (2015).
- [8] R. Verresen, F. Pollmann, and R. Moessner, Quantum dynamics of the square-lattice Heisenberg model, *Phys. Rev. B* **98**, 155102 (2018).
- [9] M. Powalski, K. P. Schmidt, and G. S. Uhrig, Mutually attracting spin waves in the square-lattice quantum antiferromagnet, *SciPost Phys.* **4**, 001 (2018).
- [10] M. R. Walther, D.-B. Hering, G. S. Uhrig, and K. P. Schmidt, Continuous similarity transformation for critical phenomena: Easy-axis antiferromagnetic XXZ model, *Phys. Rev. Res.* **5**, 013132 (2023).
- [11] G. Schmiedinghoff, L. Müller, U. Kumar, G. S. Uhrig, and B. Fauseweh, Three-body bound states in antiferromagnetic spin ladders, *Commun. Phys.* **5**, 218 (2022).
- [12] C. Knetter, K. P. Schmidt, M. Grüninger, and G. S. Uhrig, Fractional and integer excitations in quantum antiferromagnetic spin 1/2 ladders, *Phys. Rev. Lett.* **87**, 167204 (2001).
- [13] M. Windt, M. Grüninger, T. Nunner, C. Knetter, K. P. Schmidt, G. S. Uhrig, T. Kopp, A. Freimuth, U. Ammerahl, B. Büchner, and A. Revcolevschi, Observation of two-magnon bound states in the two-leg ladders of $(\text{Ca, La})_{14}\text{Cu}_{24}\text{O}_{41}$, *Phys. Rev. Lett.* **87**, 127002 (2001).
- [14] S. Notbohm, P. Ribeiro, B. Lake, D. A. Tennant, K. P. Schmidt, G. S. Uhrig, C. Hess, R. Klingeler, G. Behr, B. Büchner, M. Reehuis, R. I. Bewley, C. D. Frost, P. Manuel, and R. S. Eccleston, One- and two-triplon excitations of an ideal spin-ladder, *Phys. Rev. Lett.* **98**, 027403 (2007).
- [15] Y. Tseng, E. Paris, K. P. Schmidt, W. Zhang, T. C. Asmara, R. Bag, V. N. Strocov, S. Singh, J. Schlappa, H. M. Rønnow, S. Johnston, and T. Schmitt, Momentum-resolved spin-conserving two-triplon bound state and continuum in a cuprate ladder, *Commun. Phys.* **6**, 138 (2023).
- [16] A. W. Sandvik and J. Kurkijärvi, Quantum Monte Carlo simulation method for spin systems, *Phys. Rev. B* **43**, 5950 (1991).
- [17] A. W. Sandvik, Stochastic series expansion method with operator-loop update, *Phys. Rev. B* **59**, R14157(R) (1999).
- [18] O. F. Syljuåsen and A. W. Sandvik, Quantum monte carlo with directed loops, *Phys. Rev. E* **66**, 046701 (2002).
- [19] F. Alet, S. Wessel, and M. Troyer, Generalized directed loop method for quantum Monte Carlo simulations, *Phys. Rev. E* **71**, 036706 (2005).
- [20] A. W. Sandvik, Finite-size scaling of the ground-state parameters of the two-dimensional Heisenberg model, *Phys. Rev. B* **56**, 11678 (1997).
- [21] R. R. P. Singh, Thermodynamic parameter of the $T = 0$, spin- $\frac{1}{2}$ square-lattice Heisenberg antiferromagnet, *Phys. Rev. B* **39**, 9760 (1989).
- [22] S. Dusuel, M. Kamfor, K. P. Schmidt, R. Thomale, and J. Vidal, Bound states in two-dimensional spin systems near the Ising limit: A quantum finite-lattice study, *Phys. Rev. B* **81**, 064412 (2010).
- [23] A. W. Sandvik, Computational studies of quantum spin systems, *AIP Conf. Proc.* **1297**, 135 (2010).
- [24] H. G. Evertz, The loop algorithm, *Adv. Phys.* **52**, 1 (2003).
- [25] R. H. Swendsen and J.-S. Wang, Nonuniversal critical dynamics in Monte Carlo simulations, *Phys. Rev. Lett.* **58**, 86 (1987).
- [26] N. Kawashima and J. E. Gubernatis, Dual Monte Carlo and cluster algorithms, *Phys. Rev. E* **51**, 1547 (1995).
- [27] N. Caci, L. Weber, and S. Wessel, Hierarchical single-ion anisotropies in spin-1 Heisenberg antiferromagnets on the honeycomb lattice, *Phys. Rev. B* **104**, 155139 (2021).
- [28] L. Liu, Improvements to the stochastic series expansion method for the JQ_2 model with a magnetic field, *Phys. Rev. B* **109**, 045141 (2024).
- [29] H. Suwa and S. Todo, Generalized moment method for gap estimation and quantum Monte Carlo level spectroscopy, *Phys. Rev. Lett.* **115**, 080601 (2015).
- [30] J. D. Reger and A. P. Young, Monte Carlo simulations of the spin-1/2 Heisenberg antiferromagnet on a square lattice, *Phys. Rev. B* **37**, 5978 (1988).
- [31] A. Dorneich and M. Troyer, Accessing the dynamics of large many-particle systems using the stochastic series expansion, *Phys. Rev. E* **64**, 066701 (2001).
- [32] F. J. Dyson, General theory of spin-wave interactions, *Phys. Rev.* **102**, 1217 (1956).
- [33] S. V. Maleev, Scattering of slow neutrons in ferromagnets, *J. Exptl. Theoret. Phys. (U.S.S.R.)* **33**, 1010 (1957) [*Sov. Phys. JETP* **6**, 766 (1958)].
- [34] F. Wegner, Flow equations for Hamiltonians, *Ann. Phys. (Leipzig)* **506**, 77 (1994).
- [35] S. Kehrein, *The Flow Equation Approach to Many-Particle Systems*, Springer Tracts in Modern Physics Vol. 217 (Springer-Verlag, Berlin, 2006).
- [36] C. Knetter and G. S. Uhrig, Perturbation theory by flow equations: Dimerized and frustrated $S = 1/2$ chain, *Eur. Phys. J. B* **13**, 209 (2000).
- [37] T. Fischer, S. Duffe, and G. S. Uhrig, Adapted continuous unitary transformation to treat systems with quasi-particles of finite lifetime, *New J. Phys.* **12**, 033048 (2010).

- [38] K. Okunishi, Y. Akutsu, N. Akutsu, and T. Yamamoto, Universal relation between the dispersion curve and the ground-state correlation length in one-dimensional antiferromagnetic quantum spin systems, *Phys. Rev. B* **64**, 104432 (2001).
- [39] C. J. Hamer, Z. Weihong, and P. Arndt, Third-order spin-wave theory for the Heisenberg antiferromagnet, *Phys. Rev. B* **46**, 6276 (1992).
- [40] W. Zheng, J. Oitmaa, and C. J. Hamer, Series studies of the spin- $\frac{1}{2}$ Heisenberg antiferromagnet at $T = 0$: Magnon dispersion and structure factors, *Phys. Rev. B* **71**, 184440 (2005).
- [41] M. Kadosawa, M. Nakamura, Y. Ohta, and S. Nishimoto, Comparing quantum fluctuations in the spin- $\frac{1}{2}$ and spin-1 XXZ Heisenberg models on square and honeycomb lattices, [arXiv:2404.08099](https://arxiv.org/abs/2404.08099).
- [42] N. Caci, D.-B. Hering, M. Walther, K. P. Schmidt, S. Weßel, and G. S. Uhrig, Figure data to “Quantitative description of long-range order in the anisotropic spin-1/2 XXZ antiferromagnet on the square lattice”, Zenodo (2024), doi:[10.5281/zenodo.11189975](https://doi.org/10.5281/zenodo.11189975).
- [43] J. Cardy, *Scaling and Renormalization in Statistical Physics*, Cambridge Lecture Notes in Physics (Cambridge University Press, New York, 1996).